ELSEVIER

Catalysis Today 79–80 (2003) 169–179

CATALYSIS TODAY

www.elsevier.com/locate/cattod

# Mass transfer studies in gas–liquid–solid membrane contactors

Matevž Vospernik [a], Albin Pintar [a,*], Gorazd Berčič [a], Janez Levec [a,b]

[a] *Laboratory for Catalysis and Chemical Reaction Engineering, National Institute of Chemistry, P.O. Box 660, SI-1001 Ljubljana, Slovenia*
[b] *Department of Chemical Engineering, University of Ljubljana, P.O. Box 537, SI-1001 Ljubljana, Slovenia*

**Abstract**

This work presents a detailed study of mass transfer in gas–liquid–solid ceramic membrane contactors. For steady-state mass transfer investigations and determination of bubble-point pressure, a bench-scale low-pressure unit has been constructed for the examination of membrane contactors of various lengths. On the contrary to expectations, very low bubble-point pressure values of investigated membrane contactors were obtained, which is attributed to the presence of irregularities in the membrane wall. For the investigated range of temperatures and transmembrane pressure differences, Wilke–Chang equation provides a very good estimation for the permeance of various model compounds through the membrane wall. Rather low liquid–liquid (L–L) and gas–liquid (G–L) mass transfer rates per unit surface area of ceramic membrane tube, being in the range of $10^{-5}$ mol m$^{-2}$ s$^{-1}$, were further measured either for organic compounds dissolved in water or gases. This alludes that a gas–liquid–solid membrane contactor with a high geometric surface area should be developed in order to efficiently conduct a heterogeneously catalyzed reaction in this three-phase reactor system.


*Keywords:* Catalytic membrane reactor; Ceramic membrane contactor; Mass transfer; Bubble-point pressure measurement

## 1. Introduction

Although trickle-bed reactors are widely used in industrial three-phase processes, these systems have some disadvantages because the liquid film covering the solid catalyst pellets increases the resistance to external transfer of the gaseous reactant. This can lead to the formation of so-called preferential flow path that induces poor contact between the three phases. The presence of uncontrolled areas usually results in the formation of hot spots on the catalyst surface—a problem, which must be avoided in large-scale reactor units. This deficiency has led lately to numerous and intensive development and implementations of novel reactor types for gas–liquid–solid applications. Beside monolith reactors [1], one of the possible alternatives to the conventional trickle-bed reactor represents a membrane reactor, which has recently gained a lot of attention.

In the membrane reactor, a porous membrane used is not permselective, but it simply assures well-defined separation and contact between the gas and liquid phase flowing from opposite sides of the membrane [2]. At the same time, catalytically active phase deposited on the surface of inorganic membrane layers promotes the reaction between adsorbed reactant species. Separate feed of reactants to the membrane reactor allows independent variation of gas and liquid flow rates, reactant concentration and pressure in a wide range of operating conditions. This advantage furthermore results in additional operation flexibility and simplifies control of the membrane reactor system.

* Corresponding author. Tel.: +386-1-4760282; fax: +386-1-4760300.
*E-mail address:* albin.pintar@ki.si (A. Pintar).

0920-5861/03/$ – see front matter © 2003 Elsevier Science B.V. All rights reserved.
doi:10.1016/S0920-5861(03)00002-6

It should be pointed out that in this reactor the reaction zone is located inside the catalytically active membrane, preferentially with partially wetted active sites, which consequently increases the concentration of gaseous reactant on these sites and enhances the overall reaction rate. Such membrane reactor is classified as a catalytic nonpermselective membrane reactor or CNMR under classification of the membrane reactors, proposed by Tsotsis et al. [3].

Despite theoretical advantages and promising performance of membrane contactors over conventional three-phase reactors, relatively few publications are available in the open literature concerning hydrodynamic and reaction studies in a catalytic gas–liquid (G–L) membrane reactor. This reactor type was successfully employed in hydrogenation reactions [4,5], in ozonation of highly polluted wastewater [6,7], and for asphaltene hydrocracking [8]. Authors have studied different modes of feeding reactant solutions to the reactor unit [4,9] and an influence of transmembrane pressure difference as well as the membrane material's microstructure on ozone permeance [6,7]. However, to the best of our knowledge, no detailed investigation of mass transfer in gas–liquid–solid membrane contactors has been reported so far.

The objective of this work was thus to determine mass transfer rates in a ceramic G–L membrane contactor operating at transmembrane pressure differences lower than the bubble-point pressure. To achieve this goal, we designed and constructed a bench-scale low-pressure unit with intention of implementing these findings to investigate ceramic membranes as a possible carrier of catalytically active phase in three-phase reactions (e.g. in catalytic wet-air oxidation of organics dissolved in wastewaters as well as hydrogenation processes and production of fine chemicals), and examine possible limitations of this novel process.

## 2. Experimental

### 2.1. Ceramic membranes

The ceramic membranes used in this work were provided by TAMI industries SA (Nyons, France). Multi-layered membranes were tubular and had an internal diameter of 6 mm, an external diameter of 10 mm and total length of 10 cm. The thickest layer (thickness: 2 mm), composed of a mixture of α-alumina, zirconia and titania with a pore size in the range of 4–5 μm was placed on the outer side of the membrane. The two subsequent layers (with the thickness of 20–30 and 5 μm, respectively, and with pore size diameter in the range of 250–500 and 100–300 nm, respectively) were made of titania and titania/zirconia. The top layer made of pure rutile titania (thickness: 1–2 μm) and with pore size in the range of 5–6 nm was on the inner side of the ceramic membrane. Schematic cross-section of the membrane showing the four layers is provided elsewhere [10]. The endings of all tested membranes (1.5 cm on each side) were coated with poly(fluoroethlylenepropylene) (PFEP) or with poly(perfluoroalkoxy) (PPFA) in order to seal the ends and soften the surface on which the o-ring seals were placed. The membrane permeable active zone was thus reduced to 7 cm.

Some liquid–liquid (L–L) mass transfer and bubble-point pressure measurements were performed in the present study by employing a ceramic tubular membrane supplied by Exekia (Bazet, France). This membrane had an internal diameter of 7 mm, an outer diameter of 10 mm and total length of 35 cm. The permeable active zone of this membrane was equal to 30.7 cm. Except the thickness of the first layer, all textural properties of this membrane (i.e. radial distribution of subsequent three layers and their pore sizes) and its composition are very similar to the above described membranes.

### 2.2. Membrane characterization

Mercury-penetration method (Micromeritics Pore Sizer, model 9310) was used in order to determine total pore volume, total surface area as well as the distribution of pore volume and surface area as a function of pore diameter for tested membrane. In addition, overall porosity of a ceramic membrane tube was determined by boiling a weighed membrane sample immersed in water. In order to determine cross-sectional composition of a membrane wall, scanning electron microscopy (SEM) in back-scattering electron (BSE) mode, and energy-dispersive X-ray spectroscopy (EDX) were carried out in a Jeol 5800 scanning electron microscope equipped with the Oxford Instruments Link Isis model L300 EDX system.

For microanalysis, part of a crushed membrane tube was prepared by conventional polishing and other metallographic techniques.

### 2.3. Experimental set-up

L–L and G–L mass transfer studies were carried out in a laboratory scale membrane reactor that operated in the batch-recycle mode and is shown in Fig. 1 (Fig. 1a for L–L and Fig. 1b for G–L mass transfer studies). In this reactor set-up, a 10 cm long membrane was placed in a housing made of plexi glass in order to enable the visual observation of the processes that occur in the contactor unit (this was of particular importance for bubble-point pressure determination). The reactor was designed in such manner that one could easily switch the feed of the model compounds from the inner to the outer compartment and vice versa.

#### 2.3.1. Liquid–liquid mass transfer studies

*p*-Nitrobenzoic acid (*p*-NBA), phenol and oxalic acid were used as model compounds in L–L mass transfer studies. Experiments were performed in a wide range of operating conditions; temperature varied between 298 and 318 K, initial concentrations of model compounds were in the range of $9.3 \times 10^{-5}$ to 0.01 mol $l^{-1}$. In a typical run conducted at a transmembrane pressure difference set to 0.0 bar, an aqueous solution of a model compound was flowing through the inner compartment of the reactor, while a stream of pure distilled water was fed to the other compartment. Permeance of model compounds through the membrane wall was followed either on-line at $\lambda = 260$–275 nm by means of a UV/VIS spectrophotometer (Perkin-Elmer, model Lambda 40P) equipped with fiber optics system, or by repetitive sampling and HPLC analysis (Thermo Separations Products, model ConstaMetric 3500).

#### 2.3.2. Gas–liquid mass transfer studies

G–L mass transfer studies along with bubble-point pressure determination were conducted in a water–gas system. The G–L mass transfer studies in this apparatus were determined for water–oxygen and water–carbon dioxide systems in the temperature range of 291–298 K and at transmembrane pressure differences up to 1 bar. Gas flow rate through the apparatus was measured by means a soap film meter (Hewlett-Packard). The amount of carbon dioxide or oxygen that permeated through the membrane wall into distilled water was determined by means of a TOC analyzer (Rosemount/Dohrmann, model DC-190), or electrochemical measurements, respectively. Both possible contacting modes were tested.

1. Configuration 1: in this case gas flew through the outer compartment, while distilled water flew through the inner compartment and was recirculated in a stirred tank.
2. Configuration 2: in this case gas flew through the inner compartment, while distilled water flew through the outer compartment and was recirculated in a stirred tank.

The amount of distilled water used in each run was approximately 180 ml in configuration 1, and approximately 235 ml in configuration 2.

For the determination of bubble-point pressure values of employed ceramic membranes in a water–gas system, a UV/VIS spectrophotometer (Perkin-Elmer, model Lambda 40P) equipped with fiber optics system was used along digital camera imaging. In this examination, either argon, nitrogen or oxygen were used.

## 3. Results and discussion

### 3.1. Membrane characterization

In this investigation, part of the crushed membrane provided by TAMI was used. Fig. 2 shows SEM–BSE micrograph of the cross-sectional area of membrane wall presenting all four layers. Some irregularities (i.e. voids) can be seen in the third layer. It was found out by means of EDX microanalysis that this layer was composed of 60 wt.% $ZrO_2$, 24% $TiO_2$, 14% $Y_2O_3$ and 2% $Al_2O_3$. On the other hand, the finest inner layer contained 68 wt.% $TiO_2$ and 32% $ZrO_2$. Results obtained with mercury-penetration analysis are presented in Fig. 3, which reveals that pores smaller than 0.3 μm exhibit negligible contribution to the total pore volume and total pore surface of the examined membrane. This is in agreement with the findings of SEM analysis. It was furthermore found out by the mercury-penetration technique that the analyzed membrane contactor has a very low pore volume, i.e. 0.10 ml $g^{-1}$, and extremely low surface area of

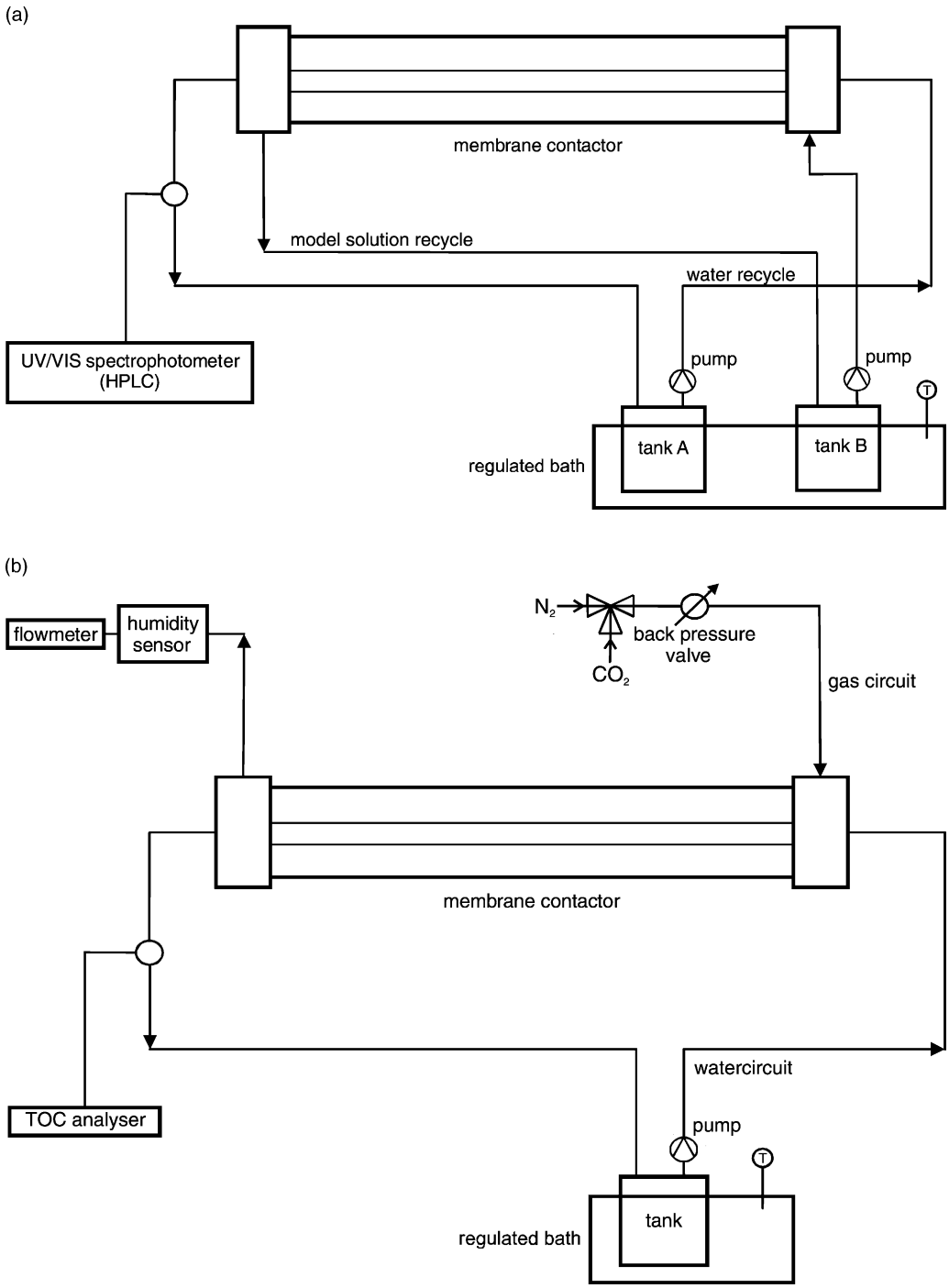


Fig. 1. Schematic drawing of a ceramic membrane contactor for (a) L–L and (b) G–L mass transfer studies.

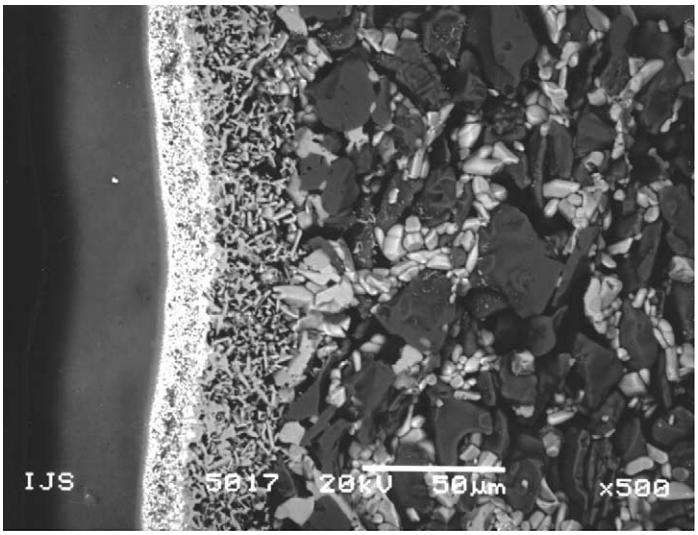


Fig. 2. Cross-sectional SEM–BSE image of four layers of the 10 cm ceramic membrane contactor.

0.12 $m^2 g^{-1}$. For our conveniences, BET surface area of the same membrane contactor was determined in parallel. The BET surface area was found to be equal to 0.3 $m^2 g^{-1}$. By means of the mercury-penetration method as well as by boiling a weighed membrane sample immersed in water, the overall porosity of membranes used in the present study was found to be in the range of 0.32–0.35.

### 3.2. Liquid–liquid mass transfer studies

Experimental results of L–L mass transfer studies obtained during the batch-recycle operating mode of 10 and 35 cm ceramic membrane contactors are presented in Fig. 4 and Table 1. One can see in Fig. 4 that temperature exhibits a positive effect on the permeance of model compound (*p*-NBA) through the membrane

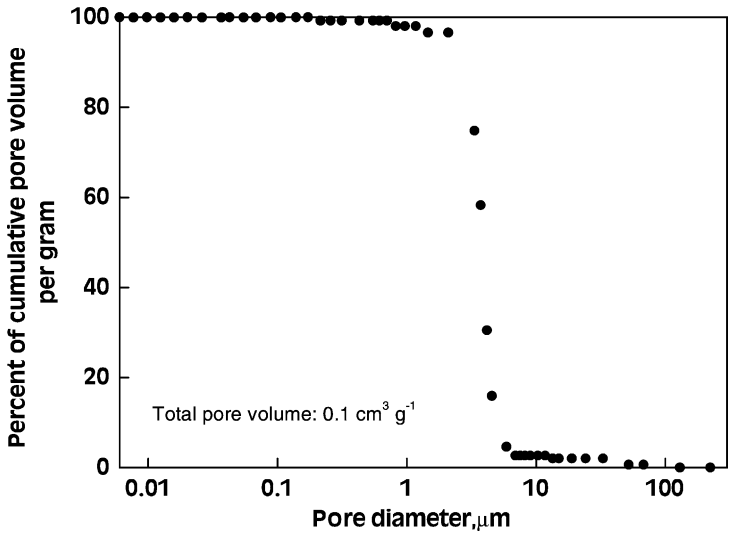


Fig. 3. Percent of cumulative pore volume as a function of pore diameter for the 10 cm ceramic membrane contactor.

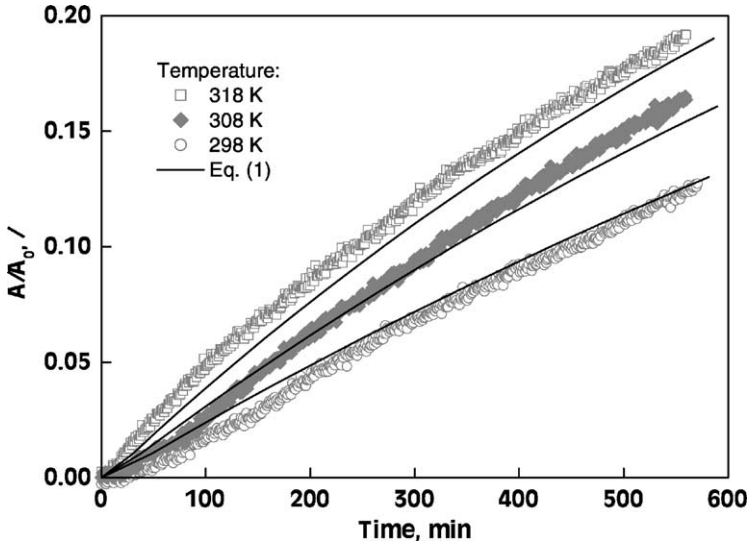


Fig. 4. Relative absorbance as a function of time obtained during L–L mass transfer studies carried out in the 35 cm ceramic membrane contactor at various temperatures. Initial solution: $9.3 \times 10^{-5}$ mol l$^{-1}$ *p*-NBA; initial absorbance ($A_0$): 0.35.

wall. On the other hand, an influence of initial concentration of model compounds on measured mass transfer rates was found to be negligible for the given range of experimental conditions. From results shown in Fig. 4 one can see that in time period of 550 min, up to 18% of *p*-NBA penetrated from the model compound solution in the inner compartment into pure water stream recycling in the outer compartment. When L–L mass transfer measurements with different model compounds were carried out in the 10 cm ceramic membrane contactor, correspondingly lower permeance values, being in the range of 3–8% of initial concentration in the same time period, were measured. On the basis of these observations, we assumed that the transport of model compounds used in the present study is governed by diffusion in pores within the membrane wall. Hence, permeance of *p*-NBA, phenol and oxalic acid through the ceramic membrane contactor was for the given range of operating conditions estimated by employing Wilke–Chang equation [11]:

$$D^0_{AB} = 7.4 \times 10^{-8} \frac{(\phi_B M_B)^{0.5} T}{\mu_B V_A^{0.6}} \quad (1)$$

where $D^0_{AB}$ is the diffusion coefficient of solute A (model compound) in solvent B (water) (m$^2$ s$^{-1}$); $M_B$ the molar mass of solvent B (g mol$^{-1}$); $\mu_B$ the viscosity of solvent B (mPa s); $T$ the temperature (K); $V_A$ the molar volume of solute (cm$^3$ mol$^{-1}$); and $\phi_B$ is the association factor for solvent B (for water $\phi_B = 2.6$).

Table 1
Diffusion coefficients and tortuosity factors for various model compounds obtained during L–L mass transfer studies carried out in the 10 cm ceramic membrane contactor ($\varepsilon = 0.32$) at $T = 318$ K

| Model compound | $c_0$ (mol l$^{-1}$) | $V_C$ (cm$^3$ mol$^{-1}$)[a] | $V_A$ (cm$^3$ mol$^{-1}$)[b] | $D^0_{AB}$ (m$^2$ s$^{-1}$)[c] | $D_{exp}/D^0_{AB}$ | $\tau$[d] |
|---|---|---|---|---|---|---|
| *p*-NBA | $1 \times 10^{-4}$ | 425.5 | 162.16 | $1.24 \times 10^{-9}$ | 0.133 | 2.40 |
| Phenol | $1 \times 10^{-4}$ | 229 | 84.7 | $1.83 \times 10^{-9}$ | 0.139 | 2.39 |
| Oxalic acid | 0.01 | 205 | 75.43 | $1.96 \times 10^{-9}$ | 0.125 | 2.56 |

[a] Critical volume (data taken from [12]).
[b] Molar volume at boiling temperature calculated by means of Eq. (2).
[c] Diffusion coefficient calculated by means of Eq. (1).
[d] Tortuosity factor.

Molar volume at boiling temperature in Eq. (1) was calculated by using the correlation proposed by Tyn and Calus [12]:

$$V_A = 0.285 \times V_C^{1.048} \quad (2)$$

where $V_C$ is the critical volume ($cm^3\,mol^{-1}$).

The values of critical volume, molar volume estimations as well as $D^0_{AB}$ coefficients are for different model compounds used in L–L mass transfer measurements collected in Table 1. In this table, values of $D_{exp}/D^0_{AB}$ coefficients are listed, which were obtained by studying L–L mass transfer of *p*-NBA, phenol and oxalic acid in the 10 cm ceramic membrane contactor operating at $T = 318$ K. From these coefficients, values of tortuosity factors were calculated. Within the accuracy of performed measurements and employed correlations very similar values were obtained, which are independent of the nature of employed model compounds. This clearly shows that the transport of compounds in ceramic membrane contactors is indeed determined by diffusion in pores within the membrane wall. Finally, the results in Table 1 again indicate that initial concentration of a model compound exhibits no influence on measured mass transfer rates.

The applicability of Wilke–Chang equation for prediction of permeance through the ceramic membrane contactor was verified also by L–L mass transfer experiments carried out in the temperature range from 298 to 318 K. Despite the 35 cm membrane tube used for this study, good agreement between measured and predicted *p*-NBA concentration versus time dependencies was obtained, as evident from Fig. 4.

### 3.3. Gas–liquid mass transfer studies

Ceramic membranes used in our study were made of hydrophilic oxide materials. So any water that came in contact with tested membranes was quickly drawn into their pores by capillary forces. Theoretical value of the capillary pressure for tested membranes can be very well estimated by means of the Laplace's equation:

$$r_p = \frac{2\gamma \cos \Theta}{\Delta P} \quad (3)$$

where $r_p$ is the radius of pores in membrane (nm); $\gamma$ the liquid–gas surface tension ($N\,m^{-1}$); $\Delta P$ the gas pressure (Pa); and $\Theta$ is the contact angle ($\Theta = 0$, for a completely wetting fluid; water contacting ceramic membrane can be assumed to fulfil this condition [6]).

#### 3.3.1. Bubble-point pressure determination

During the operation of a G–L membrane reactor, transport of the gas phase into the liquid compartment and consequent coverage of the membrane surface by gas bubbles on the liquid side should be avoided. As the applied pressure determines the location of the G–L interface within the membrane wall, determination of the so-called bubble-point pressure represents crucial information in order to find out a maximum transmembrane pressure difference in the investigated reaction system.

Configuration 2 was chosen for bubble-point pressure determinations due to the convenience of using digital camera imaging. In this study, gas pressure was gradually increased in the inner compartment from 0.0 bar to the value of bubble-point pressure. Results obtained by using the UV/VIS spectrophotometer are presented in Fig. 5. This figure clearly shows that when the bubble-point pressure value was exceeded, absorption of light and noise of signal were enhanced, which is due to the appearance of gas bubbles in water recycling in the outer compartment of ceramic membrane contactor. In comparison to theoretical bubble-point pressure values calculated by means of the Laplace's equation, surprisingly low values (in the range of 0.1–0.8 bar) were obtained experimentally for all examined membranes. So low values can be attributed either to the unequal thickness of the top layer along the membrane axial direction, or to various defects present in the membrane wall as observed in Fig. 2. The presence of defects in the membrane wall was also confirmed by these measurements, which resulted in the occurrence of non-homogeneous flux of gas into the liquid phase along the axial membrane direction, when the membrane contactor was operated at transmembrane pressure differences exceeding the bubble-point pressure.

#### 3.3.2. G–L mass transfer

When water–gas system is used in a ceramic membrane contactor, capillary forces strongly affect the liquid holdup in the membrane wall and therefore also the mass transfer of gaseous component through the membrane. When conducting G–L mass transfer studies in this system, it is favorable to put the gaseous phase on

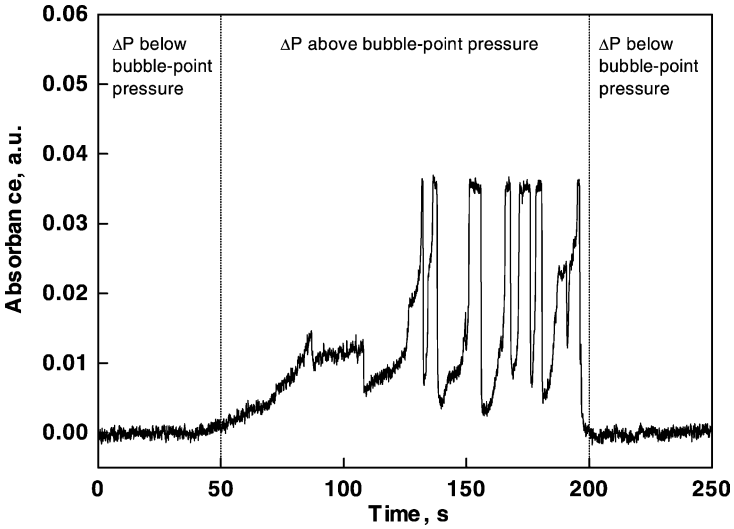


Fig. 5. Absorbance of light as a function of time obtained during the bubble-point pressure determination.

the outer membrane side (configuration 1). With this configuration one might prevent water from penetrating the ceramic membrane contactor and the consequent formation of a thin liquid film on the contactor's surface, by applying pressure of the gaseous phase that is slightly higher than hydrostatic pressure of water in inner channels of the ceramic membrane contactor. Another advantage of this configuration is that it enables control of the G–L interface within the membrane wall. Namely, in multi-layered membrane contactors the G–L interface is fixed between those layers within the membrane wall between whose respective capillary pressures the applied gas pressure is situated [7]. In comparison with gas diffusion in pores filled with a liquid, gas diffusion in dry pores is significantly higher. On account of this fact we believe that gas transfer efficiency is largely determined with the location of the G–L interface within the membrane wall. When working with an ideal membrane, this would be feasible due to their high capillary forces; however, for real membranes with considerable amount of pore defects or unfavorable textural properties, control of the G–L interface within the membrane wall is extremely pretentiousness work and it is difficult to prevent gas bubbles entering the liquid side.

In the present study, no bubble formation was observed in the experimental set-up during G–L mass transfer investigations. As can be seen from the obtained results presented in Fig. 6 and Table 2, in the measured time period of 1860 min the concentration of total inorganic carbon (TIC) in the inner compartment equals to only about 9.6% of the equilibrium concentration for $\Delta P_{CO_2} = 0.25$ bar and to only about 11.3% for $\Delta P_{CO_2} = 0.5$ bar, respectively. This shows that the permeance of $CO_2$ through the membrane

Table 2
Concentration of TIC measured after 1860 min at $T = 291$ K and various transmembrane pressure differences in the inner compartment of the 10 cm ceramic membrane contactor during G–L mass transfer studies using water–$CO_2$ system

| Medium | $\Delta P_{CO_2}$ (bar) | $c$(TIC) (mg l$^{-1}$) | $c$(TIC)/$c^*$ | $c$(TIC)/($c^*(1 + \Delta P)$) |
|---|---|---|---|---|
| Water (no pH control) | 0.25 | 38.8 | 0.096[a] | 0.077 |
| | 0.50 | 45.3 | 0.0113 | 0.075 |
| Buffer solution (pH = 6.5) | 0.25 | 50.6 | 0.083[b] | 0.066 |
| | 0.50 | 60.4 | 0.099 | 0.066 |
| Buffer solution (pH = 8.0) | 0.25 | 75.7 | 0.092[b] | 0.074 |
| | 0.50 | 91.3 | 0.111 | 0.074 |

[a] $c^*$ represents equilibrium concentration of $CO_2$ dissolved in thin water layer over the membrane surface (at applied experimental conditions, $c^* = 402$ mg l$^{-1}$ C [11]).

[b] $c^*$ represents equilibrium concentration of $CO_2$ dissolved in thin buffer film over the membrane surface. In this study, corresponding $c^*$ values were determined experimentally: $c^* = 610$ mg l$^{-1}$ C (pH = 6.5), $c^* = 820$ mg l$^{-1}$ C (pH = 8.0).

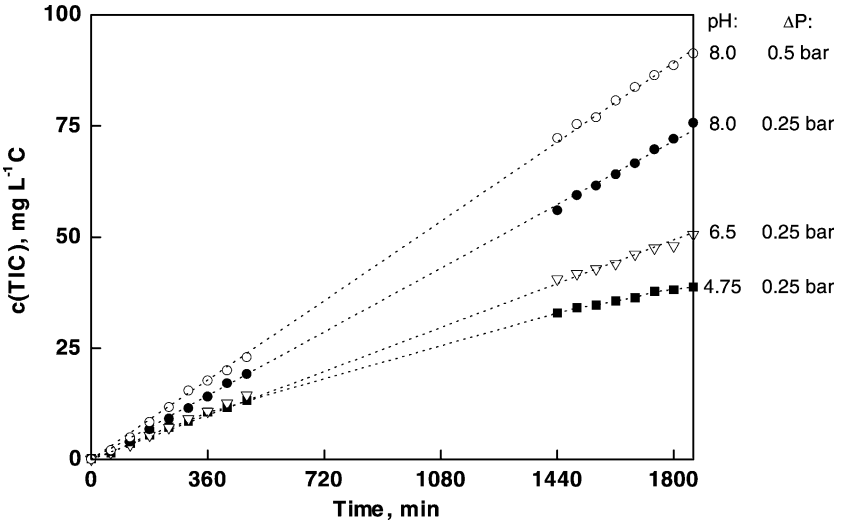


Fig. 6. Concentration of TIC as a function of time measured in the inner compartment of the 10 cm ceramic membrane contactor during the G–L mass transfer study using water–$CO_2$ system.

wall into the liquid phase was rather low. For all media used in G–L mass transfer measurements, Fig. 6 shows an increase of TIC concentration with time. When pure distilled water was recycled through the inner compartment, one can see that in the measured time period *c*(TIC) versus time curve began to bend. This was somehow expected since the gas applied in this study was $CO_2$, which resulted in pH decrease of the liquid phase (from 5.50 to 4.75) and consequently render more difficult the permeance of $CO_2$ through the membrane wall. To avoid curve bending and the influence of pH decrease on measured data (due to decrease of equilibrium concentration), further G–L mass transfer experiments were carried out in buffered solutions constituted from NaOH and $K_2HPO_4$. The results of these measurements indicate that the difference between accumulated amounts of TIC is linearly proportional to the applied transmembrane pressure (see Table 2).

On the contrary to expectations, the applied transmembrane pressure difference between the gas and liquid phase exhibited only slight influence on the permeance of carbon dioxide (or oxygen) through the membrane wall into the aqueous stream. This can be attributed to the fact that irrespectively of the applied pressure difference up to 0.8 bar, the membrane surface in the gas compartment was due to capillary forces fully covered with a liquid film in the investigated range of operating conditions. This finding is supported by data presented in Fig. 6 and Table 2, which demonstrate that the rate of carbon dioxide permeance through the membrane wall is proportional to its equilibrium concentration in the liquid film, which depends on the applied overpressure of $CO_2$ in the outer compartment and pH value of the liquid phase. It was also found out by the performed G–L mass transfer investigations that the tortuosity factor of 10 cm ceramic membrane contactor is in the range 2.25–2.55, which is in agreement with the results listed in Table 1.The fact that in the investigated range of experimental conditions the membrane surface on gas side was completely wetted at any transmembrane pressure difference, was confirmed by additional experiments in which humidity of the gas stream discharged from the ceramic membrane contactor was monitored. Fig. 7 represents relative humidity of nitrogen measured at the outlet of the membrane contactor as a function of time for two different $\Delta P$ values (one being below and the other being above the bubble-point pressure value). A detailed analysis of results illustrated in Fig. 7 reveals that a drop of relative humidity of nitrogen gas stream when increasing $\Delta P$, was due to the corresponding decrease of partial pressure of water vapor. This is confirmed by solid squares depicted in

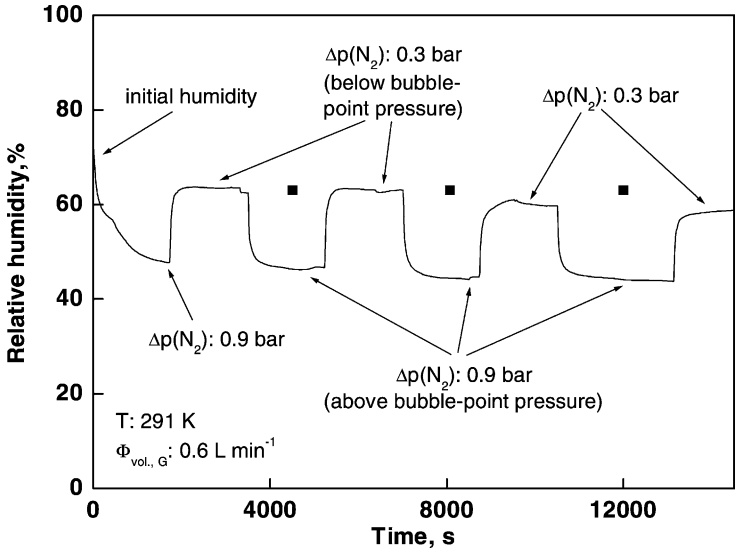


Fig. 7. Relative humidity of nitrogen as a function of time measured at the outlet of the 10 cm membrane contactor unit for various $\Delta P$ values.

Fig. 7, which were obtained by recalculating humidity data measured at $\Delta P = 0.9$ bar to $\Delta P = 0.3$ bar. On the basis of this finding, one can conclude that for the applied range of transmembrane pressure differences, G–L phase boundary in the membrane wall was not shifted. Correspondingly, in the performed G–L mass transfer investigations low permeance of carbon dioxide through the membrane wall, being in the range $7.6 \times 10^{-6}$ to $1.4 \times 10^{-5}$ mol m$^{-2}$ s$^{-1}$, was measured.

## 4. Conclusions

The results of this study demonstrate that the investigated ceramic membrane contactors exhibit very low bubble-point pressure values, which might be attributed to the presence of irregularities in the membrane wall or unfavorable textural properties of examined membrane contactors. Rather low permeance of various organic compounds or carbon dioxide through the membrane wall was observed in the investigated L–L and G–L modes of operation. It was found out that the diffusion rate of a model compound through the membrane wall is well predicted by using Wilke–Chang equation. The performed G–L measurements also demonstrate that irrespectively of the applied transmembrane pressure difference, the membrane surface on gas side was covered with a liquid film, which implies that the G–L interface did not move into the interior of ceramic membrane contactor.

In order to significantly increase mass transfer and efficiency of the investigated gas–liquid–solid membrane contactor, ceramic membranes should be developed in which G–L interface could be shifted towards thinner layers, thus ensuring shorter diffusion path.

## Acknowledgements

The authors gratefully acknowledge the financial support from the European Commission (contract No. EVK1-CT-2000-00073) and the Slovenian Ministry of Education, Science and Sport (program No. PO-0521-0104).

## References

[1] A. Cybulski, R.K. Edvinsson, S. Irandoust, B. Andersson, Chem. Eng. Sci. 48 (1993) 3463.
[2] J. Coronas, J. Santamaría, Catal. Today 51 (1999) 377.
[3] T.T. Tsotsis, R.G. Minet, A.M. Champagnie, P.K.T. Liu, in: Computer-Aided Design of Catalysts, Marcel Dekker, New York, 1993.

[4] J. Peureux, M. Torres, H. Mozzanega, A. Girord-Fender, J.-A. Dalmon, Catal. Today 25 (1995) 409.
[5] P. Cinni, M.P. Harold, Am. Inst. Chem. Eng. J. 37 (1991) 997.
[6] P. Janknecht, P.A. Wilderer, C. Picard, A. Larbot, J. Sarrazin, Chem. Eng. Technol. 23 (2000) 674.
[7] P. Janknecht, P.A. Wilderer, C. Picard, A. Larbot, J. Sarrazin, Ozone Sci. Eng. 22 (2000) 379.
[8] B. Park, V.S. Ravi-Kumar, T.T. Tsotsis, Ind. Eng. Chem. Res. 37 (1998) 1276.
[9] D. Uzio, J. Peureux, A. Girord-Fender, M. Torres, J. Ramsay, J.-A. Dalmon, Appl. Catal. A 96 (1993) 83.
[10] V. Perez, S. Miachon, J.-A. Dalmon, R. Bredesen, G. Pettersen, H. Raeder, C. Simon, Sep. Purif. Technol. 25 (2001) 33.
[11] R.H. Perry, D.W. Green, J.O. Maloney, Perry's Chemical Engineers' Handbook, seventh ed., McGraw-Hill, New York, 1997.
[12] R.C. Reid, J.M. Prausnitz, B.E. Poling, The Properties of Gases and Liquids, fourth ed., McGraw-Hill, New York, 1987.